PCCP

PAPER

View Article Online
View Journal | View Issue

Cite this: *Phys. Chem. Chem. Phys.*, 2014, **16**, 25854

The stabilities and electronic structures of single-layer bismuth oxyhalides for photocatalytic water splitting

Xue Zhang,[a] Baihai Li,*[a] Jianlin Wang,[a] Yu Yuan,[a] Qiujie Zhang,[a] Zhanzhong Gao,[a] Li-Min Liu[b] and Liang Chen[c]

Received 17th July 2014,
Accepted 13th October 2014

DOI: 10.1039/c4cp03166k

www.rsc.org/pccp

The stabilities and electronic/band structures of single-layer bismuth oxyhalides have been investigated by employing first-principles calculations. The results indicate that the single-layer bismuth oxyhalide materials, except for BiOF, have robust energetic and dynamical stabilities because of their low formation energies and the absence of imaginary frequencies within the entire Brillouin zone. Furthermore, calculations of the electronic structures and optical absorptions indicate that single-layer BiOI possesses a favorable band gap, suitable band edge positions, different orbital characteristics and different effective masses at the valence band maximum (VBM) and conduction band minimum (CBM), thus presenting excellent photocatalytic activity for water splitting. Moreover, the resulting compressive strains can shift the band edge positions of the single-layer materials to more suitable places to enhance their photocatalytic activities.

1. Introduction

As a promising way to generate hydrogen – a clean and renewable energy carrier – photocatalytic water splitting has attracted a great deal of attention because of an increasing energy crisis and environmental problems. Bismuth oxyhalides (BiOX, X = F, Cl, Br and I) have been extensively studied recently, because of their hierarchical structures and promising applications as photocatalysts for water splitting, and their ability to decompose toxic pollutants into harmless inorganic substances upon solar light irradiation.[1–6] The mechanism of photocatalytic water splitting is illustrated in Fig. 1(a). The electrons are excited from the valence bands to the conduction bands by the incident sunlight, leading to the formation of electron–hole pairs. Subsequently, the photo-generated electrons and holes can participate in hydrogen and oxygen generation reactions according to the two chemical reactions – H_2: $2H^+ + 2e^- = H_2$, O_2: $H_2O = 1/2O_2 + 2H^+ + 2e^-$, respectively. Two conditions must be satisfied for a promising photocatalyst. First, the width of the band gap of a candidate has to exceed the free energy of water splitting of 1.23 eV.[7] Second, the conduction band minimum (CBM) must be higher than the reduction potential of H^+/H_2 (−4.44 eV at pH = 0), and the valence band maximum (VBM) must be lower than the oxidation potential of O_2/H_2O (−5.67 eV at pH = 0).[8,9]

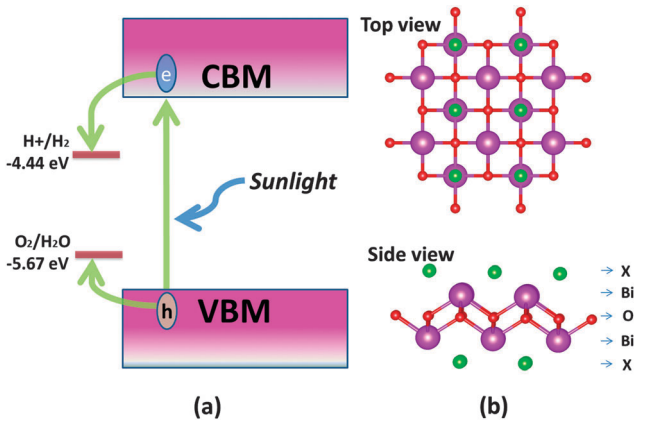

Fig. 1 (a) Illustration of the mechanism of photocatalytic water splitting; (b) top and side view of the geometric structure of single-layer BiOX.

The lamellar structures of BiOX with interleaved atomic-layered $[Bi_2O_2]^{2+}$ and halogen X atom slabs along the *c* direction are constructed by strong intra-layer electric fields within the BiOX slabs and weak van der Waals bonds between the two closely adjacent halogen X slabs.[4,5] The internal electric fields formed between $[Bi_2O_2]^{2+}$ and the halogen atom layers can remarkably accelerate the transport and reduce the recombination rate of the electron–hole pair, leading to a high photocatalytic activity.[3,10] Promoted by the novel mechanical and electronic properties of 2D materials, a great deal of studies

[a] School of Energy Science and Engineering, University of Electronic Science and Technology of China, Chengdu 611731, China. E-mail: libaihai.uestc@gmail.com
[b] Beijing Computational Science Research Center, Beijing, 100084, P. R. China
[c] Ningbo Institute of Materials Technology and Engineering, Chinese Academy of Sciences, Ningbo 315201, China

have been performed to explore the synthetic methodologies and potential applications of BiOX nanosheets or nanoplates.[1,11] For instance, it has also been demonstrated that all BiOCl, BiOBr and BiOI nanoplates exhibit more superior activity than commercial TiO_2 (P25, Degussa) towards methyl orange (MO) dye degradation under UV-visible light irradiation, and that BiOI is the best photocatalyst with a degradation efficiency reaching 80% in 3 hours under visible light illumination.[12] The experiments performed by Yu *et al.* have evidenced that BiOI possesses higher photocatalytic activity than Bi_5O_7I and Bi_2O_3 under visible light irradiation.[13] The higher photocatalytic activity of BiOI is attributed to its narrower band gap. Moreover, the heterostructure BiOI/BiOBr[14] and the solid solution xBiOBr–$(1-x)$BiOI[15] have been synthesized to enhance photocatalytic performances. Indeed, those composite materials showed higher activities than that of the individual component for the degradation of MO under visible light. A new bismuth-based material, $Bi_{24}O_{31}Br_{10}$ is thought of as an important photocatalyst with a remarkable reduction activity to generate hydrogen from water under visible-light irradiation.[16] BiOCl with a wide band gap has attracted considerable attention, because of its high activity and high stability. Zhao and co-workers[3] revealed that the photocatalytic activity of BiOCl single-crystalline nanosheets is surface dependent. The BiOCl (001) surface has a higher activity in direct semiconductor photoexcitation pollutant degradation under UV light, while the (010) surface exhibits a higher activity in indirect dye photosensitization degradation under visible light. The photocatalytic activities of noble metal decorated BiOX investigated by Yu *et al.* have shown that the deposition of the noble metal can enhance the visible light absorption and improve the photocatalytic performance.[17]

Many atomically-thick materials have shown outstanding properties and tremendous potential applications. For instance, Wang and co-workers[18] suggested that graphene oxide can be used as an ideal substrate for hydrogen storage. Small concentration hole-doping into a graphene-like MnO single layer leads to a switch from antiferromagnetism into a half-metallic ferromagnetic configuration.[19] Xiang's group[20] predicted a stable 2D boron–carbon compound BC_3 which exhibits a semiconductor behavior. Moreover, Liu and co-workers[21] proposed that single-layer metal phosphorus trichalcogenides are potential photocatalysts for overall water splitting. Inspired by these progressive achievements, we thus expect that single-layer BiOX could also be obtained through mechanical or chemical exfoliation strategies, and could exhibit highly efficient photocatalytic performance. Therefore, it is important to perform a comprehensive investigation on the stabilities and electronic structures of single-layer BiOX materials. To the best of our knowledge, the study of the properties of single-layer BiOX is rather limited.

In this work, we attempt to study single-layer BiOX by employing first-principles calculations. First, the stabilities of the materials were investigated according to the formation energies and the phonon spectrum analysis. Subsequently, the feasibility of the single-layer BiOX materials for use as photocatalysts for water splitting was studied based on the calculated electronic structures. Finally, we explored the efficiency of the mechanical strains by adjusting the band gaps and band edge positions of single-layer BiOX to enhance their photocatalytic activity.

2. Computational methods

First-principles calculations were performed using the Vienna *Ab initio* Simulation Package (VASP).[22] Projector-augmented-wave (PAW) potentials[23] were used for the treatment of the core electrons. The electron exchange correlation interactions were treated within the generalized gradient approximation (GGA) using the Perdew–Burke–Ernzerhof (PBE) functional.[24] To ensure that the interactions between the slabs along the vertical direction are negligible, a vacuum layer with a total thickness of 30 Å was set at both sides of the respective atomic layer. A soft oxygen pseudopotential with a valence configuration of $2s^2 2p^4$ and a default cutoff energy of 250 eV was adopted in the calculations. In order to check the accuracy of the calculations, the phonon of BiOCl was also checked with 500 eV, and the results show that the higher energy cutoff gives the same result as that of the 320 eV cutoff. The energy cutoff was set to 320 eV and the k-point sampling of $7 \times 7 \times 1$ utilized the Monkhorst–Pack[25] scheme. Equilibrium geometries were obtained by fully optimizing both the atom positions and lateral lattice vectors to a tolerance of less than 0.02 eV $Å^{-1}$ on each atom. To study the stabilities of BiOX, we performed phonon calculations using the supercell approach.[26] Force constants and phonon frequencies were calculated using the PHONOPY code.[27]

The electronic structures of single-layer BiOX were calculated by HSE06[28–30] methods to overcome the deficiency of standard DFT in describing the exchange–correlation (XC) energy. The exact exchange contribution is represented by a value of 25% HF and 75% PBE contributions. The work functions were calculated, and then the CBM and VBM were placed at the positions referring to the vacuum level, according to[31,32]

$$E_{\mathrm{CBM/VBM}} = E_{\mathrm{BGC}}^{\mathrm{HSE06}} \pm \tfrac{1}{2}E_g^{\mathrm{HSE06}} \quad (1)$$

where the band center energy, E_{BGC}, and the band gap were calculated by the HSE06 method.

3. Results and discussion

3.1 Geometric structure and stabilities

The structures of single-layer BiOX were illustrated in Fig. 1(b). Upon relaxation by PBE-based DFT calculations, the lateral lattice constants $a = b$ for single-layer BiOX were optimized to be 3.711, 3.889, 3.930, and 4.014 Å, which are very close to the experimental values of 3.748, 3.89, 3.916 and 3.985 Å for BiOF, BiOCl, BiOBr and BiOI unit bulks,[33] respectively. The subtle differences in the lattice parameters indicate that ideally isolated single-layer BiOX slabs can keep their geometric integrity and experience negligible relaxation or construction. The binding interactions of a single atom in the halogen X slabs with $[Bi_2O_2]^{2+}$ slabs were determined according to

$$E_{\mathrm{b}} = (E_{\mathrm{BiOX}} - E_{\mathrm{BiO}} - E_{\mathrm{X}})/n \quad (2)$$

where E_{BiOX}, E_{BiO} and E_X are the total energies of BiOX, $[Bi_2O_2]^{2+}$ and the halogen X slabs, respectively, and n is the number of atoms in the halogen X slabs. The calculated values are −5.77, −4.13, −3.52 and −2.74 eV per atom for BiOF, BiOCl, BiOBr and BiOI, respectively, indicating the typical chemical bonding interactions between the halogen X atoms and the $[Bi_2O_2]^{2+}$ slabs.

Subsequently, we evaluated the interactions between two adjacent BiOX slabs *via* the calculations of the formation energies of single-layer BiOX, according to the formula:[31]

$$E_f = E_{2D}/N_{2D} - E_{3D}/N_{3D} \quad (3)$$

where E_{2D} and E_{3D} are the energies of the single-layer and 3D bulk BiOX, and N_{2D} and N_{3D} are the numbers of atoms in their unit cells, respectively. In order to ensure the accuracy of the description of the interactions between atomic layers, four different functionals were adopted for the calculations of the formation energies of the single-layer BiOX materials. The results were compared in Fig. 2. We first performed PBE functional based conventional DFT calculations to evaluate the formation energies. The value for single-layer BiOF is calculated to be 0.06 eV per atom, which is significantly smaller than the energy of F atoms binding with the $[Bi_2O_2]^{2+}$ slab, indicating that single-layer BiOF might be easily exfoliated from the bulk BiOF. Moreover, the negative values of −0.0006 (almost naught), −0.02 and −0.06 eV per atom for the formation energies of single-layer BiOCl, BiOBr and BiOI suggest that the ground states of the three atomically-thick materials could be more stable than their 3D counterparts, and thus may be formed spontaneously. More accurate HSE06 functionals were then used to verify the results obtained by the PBE functional based calculations. The calculations show that the HSE06 method yields slightly positive formation energies of 0.12, 0.004, −0.008 and −0.03 eV per atom for single-layer BiOF, BiOCl, BiOBr and BiOI respectively. Since the values of single-layer BiOBr and BiOI are calculated to be negative by both the PBE and HSE06 methods, it is implied that the two materials might be stable in a 2D morphology. Nevertheless, note that the interactions between two adjacent single-layer BiOX slabs are weak; it is necessary to take the dispersive electrostatic interactions between halogen X atom slabs into consideration. We thus performed PBE + vdW and HSE06 + vdW calculations, by employing the DFT-D2 method of Grimme,[34] on the total energies of these structures to determine the feasibility of single-layer BiOX formation. In this way, all of the formation energies are calculated to be slightly positive. The formation energy of BiOF calculated by the HSE06 + vdW method is still the largest one with a value of 0.16 eV per atom. Similarly, the formation energies of single-layer BiOCl, BiOBr and BiOI calculated by the PBE + vdW and HSE06 + vdW methods are comparable to the values for single-layer GaS, GaSe, and MoS_2,[31] which have already been successfully obtained by mechanical exfoliation or chemical synthesis.[35–37] Therefore, we expect that the single-layer BiOX materials can feasibly be obtained by cleaving from their 3D counterparts, except for BiOF because of its relatively high formation energy. Overall, our extensive calculations showed that the intra-layer interactions between X atoms and the $[Bi_2O_2]^{2+}$ slab within the single-layer BiOX are significantly stronger than the inter-layer interactions between two adjacent BiOX sheets in the 3D bulk structures.

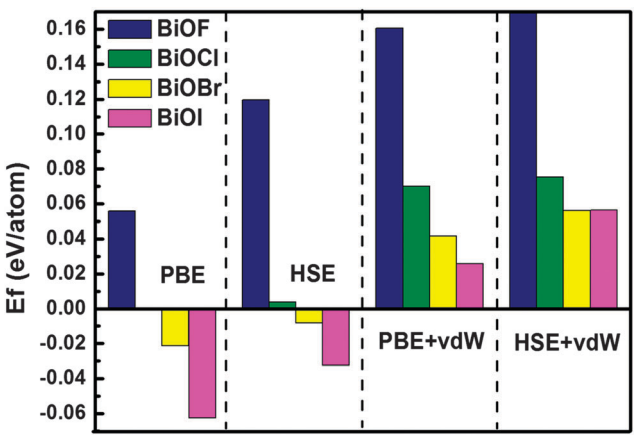

Fig. 2 The formation energies of single-layer BiOX (X = F, Cl, Br, I).

Phonon dispersion spectrum analysis is a reliable method for the verification of the stabilities of single-layer BiOX. Its requisite for a stable structure to meet the condition is that all of its phonon frequencies on the *k*-points in the Brillouin zone should be positive.[38,39] As shown in Fig. 3, no imaginary vibration frequency appears in the phonon band spectra for single-layer BiOCl, BiOBr and BiOI (see Fig. 3(b)–(d)), which indicates that the structures have a high phonon stability. However, the evidenced imaginary frequency on the phonon spectrum of BiOF demonstrates that this material is an unstable single-layer material (see Fig. 3(a)), and thus is difficult to prepare.

3.2 Electronic structures

Since single-layer BiOF is not stable, it is not necessary to further investigate its band/electronic structures. The band structures of the rest of the single-layer BiOX (henceforth, X = Cl, Br and I) materials calculated by the HSE06 functional, shown in Fig. 4, indicate that all the BiOX materials exhibit indirect band gaps with the CBM located at the *Z* points and the VBM located between the *R* and *Z* points in the irreducible Brillouin zone (IBZ). As suggested by Zhang and co-workers,[40] the indirect band gap characteristic helps to reduce the recombination rate of photo-generated carriers, in that the excited electrons must emit a phonon during the transition back to the valence band with a certain *k*-space distance to travel. But we must note that the indirect band gap also makes the material a poor absorber of light. The itinerancy of the electrons increases in the order of the atomic number of the halogen atom in single-layer BiOX, which gives a reason for the decrease of the band gaps in the order of BiOCl > BiOBr > BiOI, with the calculated values of 3.79, 3.41 and 2.3 eV, respectively. Because of the quantum size effect, the band gaps of single-layer BiOX are larger than the values of 3.47, 2.84 and 1.87 eV for BiOCl, BiOBr and BiOI,[17] respectively. The band gaps indicate that the single-layer BiOCl and BiOBr

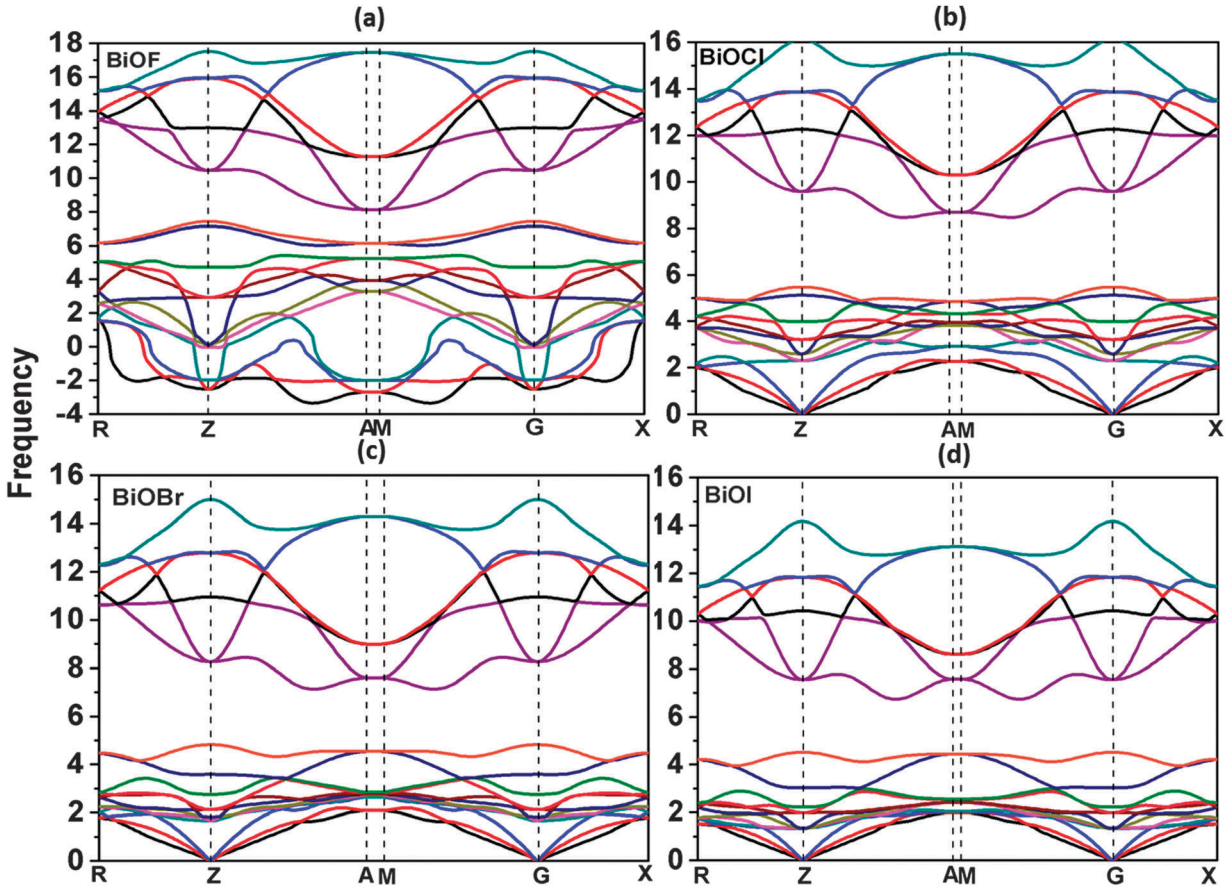

Fig. 3 The phonon dispersion spectrum of single-layer BiOX (X = F, Cl, Br, I).

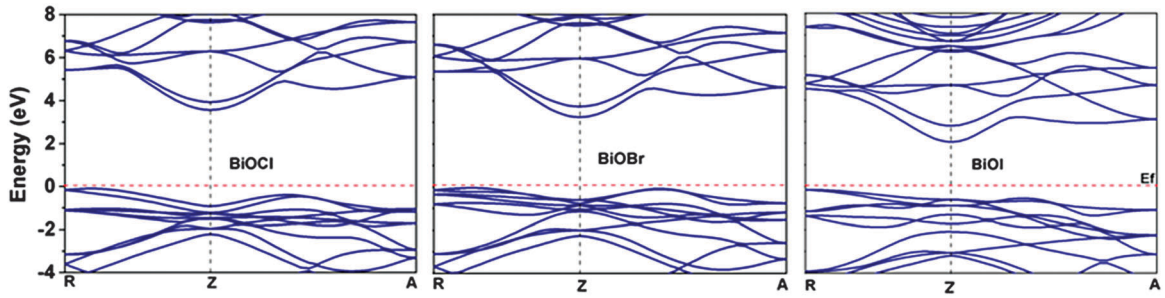

Fig. 4 The band structures of single-layer BiOCl, BiOBr and BiOI, respectively. The Fermi level is set to 0 eV.

materials might only be activated under UV light, while the BiOI material can absorb visible light of the solar spectrum. Therefore, the single-layer BiOI material is expected to be the best photocatalyst candidate for water splitting among these BiOX materials. Single-layer BiOI with a band gap of 2.3 eV is appropriate for the photocatalytic water splitting reaction, which requires at least ~1.9–2.0 eV.[41,42] Furthermore, the distinctively dispersive feature at the band edges implies that photo-generated carriers should have a high carrier mobility. We thus estimate the effective masses of the electron and hole by fitting the dependence relationship of the energy to wave vector at the VBM and CBM. The effective masses for BiOCl, BiOBr and BiOI at the CBM (m_e*) are calculated to be 0.56, 0.48 and 0.40 m_e along $R \rightarrow Z$, respectively, indicating that the electron has excellent mobility, even better than that in anatase TiO_2 (m_e* = 1 m_e).[43] On the other hand, as for the photo-generated hole, the diffusion in the valence bands is relatively weak, because the hole effective masses for BiOCl, BiOBr and BiOI at the VBM (m_h*) are calculated to be 1.10, 1.05 and 2.75 m_e along $R \rightarrow Z$, respectively, which are much larger than those values of the electrons at the CBM. The significant difference between the m_e* and the m_h* indicates the great difference in the mobility of the carriers and the resulting lower recombination rate of the electron–hole pairs.[44] Note that a high diffusion rate and long lifetime of the carriers are distinctly important for high-efficiency photocatalysts.

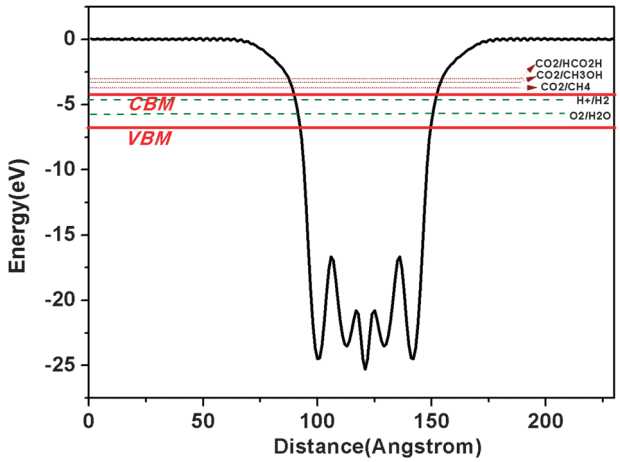

Fig. 5 The CBM and VBM of single-layer BiOI relative to the redox potentials of the water splitting reactions and the CO_2 reduction reactions producing methane, methanol and formic acid at pH = 0. The bold black line represents the average electrostatic potential calculated with the HSE06 functional.

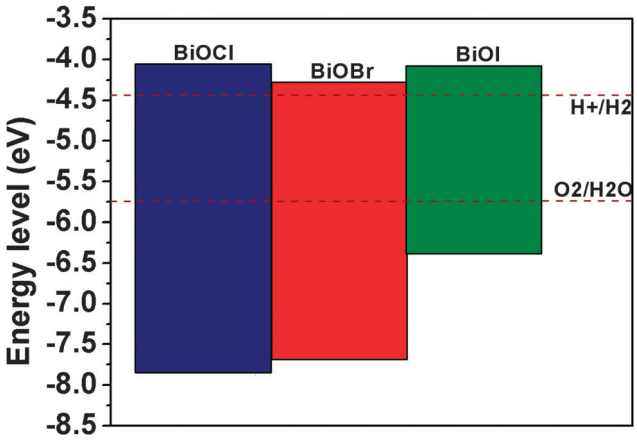

Fig. 6 Comparison between the band edge positions of single-layer BiOCl, BiOBr and BiOI related to the vacuum level calculated with the HSE06 functional and the standard redox potentials for water splitting at pH = 0.

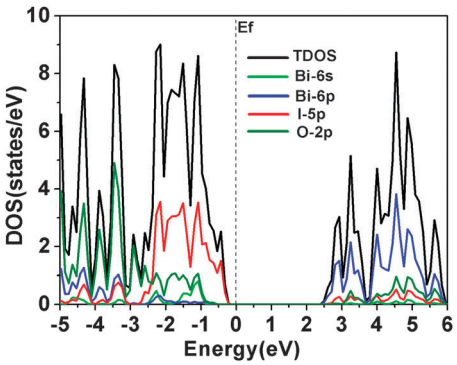

Fig. 7 The total and partial density of states (DOS) of single-layer BiOI.

In order to catalyze the water splitting reaction, the positions of the CBM and VBM must straddle the redox potential of water. We first performed work function calculations upon these single-layer BiOX materials with a HSE06 functional, and then placed the CBM and VBM at certain positions with respect to the vacuum level to determine the photocatalytic capability, as suggested by Zhuang.[31] For BiOCl, BiOBr and BiOI, the work functions are calculated to be 7.94, 7.83 and 6.65 eV, respectively. Taking single-layer BiOI as an example, as shown in Fig. 5, the CBM lies higher in energy than the reduction potential of H^+/H_2 and its VBM energy is lower than the oxidation potential of O_2/H_2O, which indicates that single-layer BiOI is appropriate for the photocatalytic water splitting reaction. In addition, the results indicate that it is unfeasible to catalyze the reduction reactions of CO_2 to produce methane, methanol and formic acid, because the CBM of BiOI is lower than the reduction potentials of CO_2.

The comparison of the CBM and VBM energy levels with the redox potentials of water splitting in Fig. 6 shows that all of the single-layer BiOX materials have band edges situated in energetically favorable positions for water splitting. The results indicate that the three single-layer BiOX materials are appropriate for catalyzing the overall water splitting.

The density of states (DOS) of BiOI was taken as an example to understand the bonding characteristics of single-layer BiOX, as shown in Fig. 7. The valence band (VB) top is occupied by I-5p states, within the energy of −2.0 to −0.5 eV the orbits of O-2p and Bi-6s are clearly presented, although the amplitude are much lower; and the bonding states locating between −5.0 and −3.0 eV are formed by Bi-6p and O-2p with some contributions from I-5p. Nevertheless, the conduction band (CB) bottom mainly derives from the Bi-6p states with minor contributions from the I and O atoms. It is thus reasonable to expect that the conduction and valence band edges with different characteristics can help to substantially reduce the photo-generated electron–hole recombination rates. Bader charge analysis[45] shows that each Bi atom donates 2.95 electrons, while each I and O obtain 0.59 and 2.36 electrons, respectively, representing the strong chemical bonding interactions within the atomic BiOX layers.

3.3 Optical absorption

It is well known that the interactions between a photon and an electron system can be interpreted in terms of the time-dependent perturbations of the ground-state electronic states. The optical spectra caused by the interband transitions of excitations from the occupied to the unoccupied states can be described as a joint density of states between the valence and conduction bands. The dielectric function, $\varepsilon(\omega)$ is an important aspect of the optical properties. Considering the appropriate transition momentum matrix elements, the imaginary part of the dielectric function, $\varepsilon_2(\omega)$ is calculated by summing all possible transitions from the unoccupied to the occupied wave functions within the selection rules.[46] The real part of the dielectric function, $\varepsilon_1(\omega)$ can be derived from $\varepsilon_2(\omega)$ using the Kramer–Kronig relationship. Therefore, the absorption

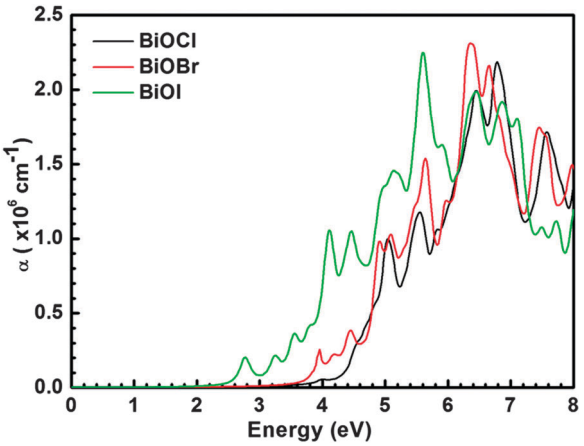

Fig. 8 The calculated optical absorption spectra of single-layer BiOX using the HSE06 method.

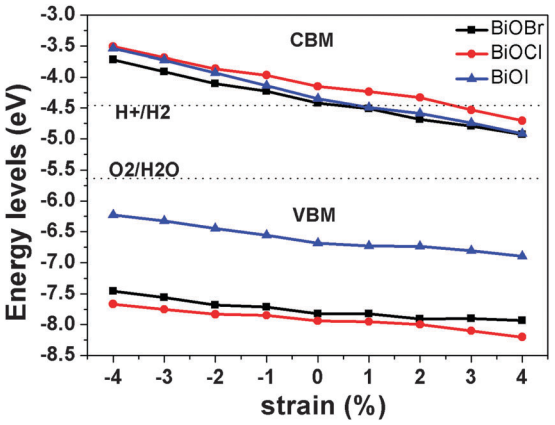

Fig. 9 The effect of strain on the band edge positions of single-layer BiOX.

coefficient $\alpha(\omega)$ can be calculated from the dielectric components $\varepsilon_1(\omega)$ and $\varepsilon_2(\omega)$ using the following expression:

$$\alpha(\omega) = \sqrt{2}\omega\left[\sqrt{\varepsilon_1^2(\omega) + \varepsilon_2^2(\omega)} - \varepsilon_1(\omega)\right]^{1/2} \quad (4)$$

The calculated optical absorption spectra of single-layered BiOX using the HSE06 functional are shown in Fig. 8. The absorption is activated by the irradiation with energies larger than 3.82, 3.41 and 2.43 eV for BiOCl, BiOBr and BiOI, respectively, which are very close to the values of the indirect band gaps. The transition of electrons from the *R* point at the VBM to the *Z* point at the CBM needs the assistance of the phonon, resulting in the weak absorption of the visible light represented by the gentle edge of the spectrum. The first peaks around 3.8 eV and 2.7 eV on the respective absorption spectra of BiOBr and BiOI can be attributed to the direct transition of electrons at the *Z* point of the Brillouin zone. There is no remarkable peak around 4.2 eV on the absorption spectrum of BiOCl, which is corresponding to the energy difference between its valence and conduction band edges at the *Z* point. On the contrary, the absorption coefficient rises rapidly to the order of 10^6 cm^{-1} at about 5.0 eV. We assume that the representative characteristic of absorption for BiOCl is a result of the collective contribution from the direct and/or indirect interband transitions at high-symmetry points and/or axes in the Brillouin zone, caused by the incident photon with an appropriate energy. The noise in the absorption spectra could result from the anisotropic band structures and a small width of smearing in the calculations in order to achieve high precision.

3.4 Strain effects

As mentioned above, the suitable width of the band gap and the appropriate band edge positions are two critical factors to efficiently harvest solar energy. However, the band gaps of BiOCl and BiOBr are too large, leading to low photocatalytic efficiency to absorb sun light. In addition, the positions of the CBMs for the three single-layer BiOX materials are just slightly over the reduction potential level for water splitting, implying that the reduction potential of the photo-generated electrons might not be sufficient to produce hydrogen from water. A valid method to solve these problems is through band gap engineering by applying strains.[47] The epitaxial growth on suitable substrates, in practice, is an effective way to realize these strains.[31]

Biaxial strains in the range from −4% to +4% were applied on the single-layer BiOX to explore the effects of the strain on the band gaps and band edge positions. The HSE06 functional was employed to relax the atomic coordinates to the equilibrium positions at each biaxial strain and then calculate the corresponding band structures. The variation of the CBM and VBM of the single-layer BiOX with strains, as shown in Fig. 9, provides important guidance for tuning the CBM and VBM levels of the single-layer BiOX to maximize the efficiency of the photocatalysis. There is little change for the band gaps upon the applied strains, while the position adjustment of the CBM and VBM levels depends linearly on the strain. Specifically, the band edge positions of all single-layer BiOX materials are shifted upwards to higher positions with respect to the redox potential level of water at compressive strains. The positions of the CBMs were elevated much faster than those of the VBMs during the compression process. Thus, the photo-generated electrons could be endowed with a stronger reduction capability to generate hydrogen from water. Conversely, tensile strains make the band edge positions of all these three materials unfavorable for water splitting, due to the positions of the CBMs, which are enforced below the reduction potential of H^+/H_2.

4. Conclusion

We have comprehensively investigated the stabilities and electronic structures of single-layer BiOX materials and explored the potential of the materials for photocatalytic water splitting. Negative or low positive formation energies obtained by different

approaches indicate that single-layer BiOCl, BiOBr and BiOI can be feasibly obtained by mechanical exfoliation. Furthermore, phonon dispersion spectra analyses verified the stabilities of single-layer BiOCl, BiOBr and BiOI, but not BiOF. The calculations of the band structures performed with the HSE06 functional suggest that the single-layer BiOX (X = Cl, Br, I) materials are promising photocatalysts for water splitting. Notably, the band gap of single-layer BiOI is 2.3 eV, indicating that the atomically-thick material can respond to visible light. The different orbital characteristics and different effective masses at the valence band maximum (VBM) and the conduction band minimum (CBM) are important factors for a high-efficiency photocatalyst. However, the optical property calculations indicated that the absorption of visible light is relatively weak because of the indirect band gaps of the single-layer BiOX. In addition, we explored the effects of mechanical strains on the adjustment of the band gaps and band edge positions. Our calculations show that compressive strains on BiOCl, BiOBr and BiOI can increase the band gaps slightly but render the band edge positions to be more favorable for hydrogen production, and thus enhance the efficiency of the photocatalytic activities of BiOCl, BiOBr and BiOI.

Acknowledgements

We acknowledge the financial support by the national science foundation of China (Grant No. 51472254, 11104287 and 11105129), technology innovative research program of Ningbo (Grant No. 2011B82005) and Ningbo NSF (Grant No. 2012A610099 and 2012A610117).

References

1 J. Jiang, K. Zhao, X. Xiao and L. Zhang, *J. Am. Chem. Soc.*, 2012, **134**, 4473–4476.
2 M. Guan, C. Xiao, J. Zhang, S. Fan, R. An, Q. Cheng, J. Xie, M. Zhou, B. Ye and Y. Xie, *J. Am. Chem. Soc.*, 2013, **135**, 10411–10417.
3 K. Zhao, L. Zhang, J. Wang, Q. Li, W. He and J. J. Yin, *J. Am. Chem. Soc.*, 2013, **135**, 15750–15753.
4 H. Cheng, B. Huang and Y. Dai, *Nanoscale*, 2014, **6**, 2009–2026.
5 L. Ye, Y. Su, X. Jin, H. Xie and C. Zhang, *Environ. Sci.: Nano*, 2014, **1**, 90–112.
6 W. Su, J. Wang, Y. Huang, W. Wang, L. Wu, X. Wang and P. Liu, *Scr. Mater.*, 2010, **62**, 345–348.
7 K. Maeda and K. Domen, *J. Phys. Chem. C*, 2007, **111**, 7851–7861.
8 S. Trasatti, *Pure Appl. Chem.*, 1986, **58**, 955–966.
9 D. K. Kanan and E. A. Carter, *J. Phys. Chem. C*, 2012, **116**, 9876–9887.
10 H. Cheng, B. Huang and Y. Dai, *Nanoscale*, 2014, **6**, 2009–2026.
11 H. Li, Q. Jia, Y. Cui and S. Fan, *Mater. Lett.*, 2013, **107**, 262–264.
12 X. Zhang, Z. Ai, F. Jia and L. Zhang, *J. Phys. Chem. C*, 2008, **112**, 747–753.
13 C. Yu, C. Fan, J. C. Yu, W. Zhou and K. Yang, *Mater. Res. Bull.*, 2011, **46**, 140–146.
14 J. Cao, B. Xu, B. Luo, H. Lin and S. Chen, *Catal. Commun.*, 2011, **13**, 63–68.
15 W. Wang, F. Huang, X. Lin and J. Yang, *Catal. Commun.*, 2008, **9**, 8–12.
16 J. Shang, W. Hao, X. Lv, T. Wang, X. Wang, Y. Du, S. Dou, T. Xie, D. Wang and J. Wang, *ACS Catal.*, 2014, **4**, 954–961.
17 C. Yu, F. Cao, G. Li, R. Wei, J. C. Yu, R. Jin, Q. Fan and C. Wang, *Sep. Purif. Technol.*, 2013, **120**, 110–122.
18 L. Wang, K. Lee, Y.-Y. Sun, M. Lucking, Z. Chen, J. J. Zhao and S. B. Zhang, *ACS Nano*, 2009, **3**, 2995–3000.
19 E. Kan, M. Li, S. Hu, C. Xiao, H. Xiang and K. Deng, *J. Phys. Chem. Lett.*, 2013, **4**, 1120–1125.
20 X. Luo, J. Yang, H. Liu, X. Wu, Y. Wang, Y. Ma, S.-H. Wei, X. Gong and H. Xiang, *J. Am. Chem. Soc.*, 2011, **133**, 16285–16290.
21 J. Liu, X.-B. Li, D. Wang, W.-M. Lau, P. Peng and L.-M. Liu, *J. Chem. Phys.*, 2014, **140**, 054707.
22 G. Kresse and J. Hafner, *Phys. Rev. B: Condens. Matter Mater. Phys.*, 1993, **48**, 13115–13118.
23 P. E. Blochl, *Phys. Rev. B: Condens. Matter Mater. Phys.*, 1994, **50**, 17953–17979.
24 J. Perdew, J. A. Chevary, S. H. Vosko, K. Jackson, M. Pederson, D. J. Singh and C. Fiolhais, *Phys. Rev. B: Condens. Matter Mater. Phys.*, 1992, **46**, 6671–6687.
25 H. J. Monkhorst and J. D. Pack, *Phys. Rev. B: Solid State*, 1976, **13**, 5188.
26 A. Togo, F. Oba and I. Tanaka, *Phys. Rev. B: Condens. Matter Mater. Phys.*, 2008, **78**, 134106.
27 A. Togo, Phonopy, http://phonopy.sourceforge.net/.
28 J. Heyd, G. E. Scuseria and M. Ernzerhof, *J. Chem. Phys.*, 2003, **118**, 8207.
29 J. Paier, M. Marsman, K. Hummer, G. Kresse, I. C. Gerber and J. G. Ángyán, *J. Chem. Phys.*, 2006, **125**, 249901.
30 N. Seriani, W. Pompe and L. C. Ciacchi, *J. Phys. Chem. B*, 2006, **110**, 14860–14869.
31 H. L. Zhuang and R. G. Hennig, *Chem. Mater.*, 2013, **25**, 3232–3238.
32 M. C. Toroker, D. K. Kanan, N. Alidoust, L. Y. Isseroff, P. Liao and E. A. Carter, *Phys. Chem. Chem. Phys.*, 2011, **13**, 16644–16654.
33 R. W. G. Wyckoff, *Crystal Structures*, John Wiley & Sons, Inc., New York, 2nd edn, 1963, vol. 1.
34 S. Grimme, *J. Comput. Chem.*, 2006, **27**, 1787–1799.
35 K. Novoselov, D. Jiang, F. Schedin, T. Booth, V. Khotkevich, S. Morozov and A. Geim, *Proc. Natl. Acad. Sci. U. S. A.*, 2005, **102**, 10451–10453.
36 P. Hu, L. Wang, M. Yoon, J. Zhang, W. Feng, X. Wang, Z. Wen, J. C. Idrobo, Y. Miyamoto and D. B. Geohegan, *Nano Lett.*, 2013, **13**, 1649–1654.
37 P. Hu, Z. Wen, L. Wang, P. Tan and K. Xiao, *ACS Nano*, 2012, **6**, 5988–5994.

38 Q. Li, D. Zhou, W. Zheng, Y. Ma and C. Chen, *Phys. Rev. Lett.*, 2013, **110**, 136403.
39 W. Yin, Y. Xie, L. Liu, R. Wang, X. Wei, L. Lau, J. Zhong and Y. Chen, *J. Mater. Chem. A*, 2013, **1**, 5341–5346.
40 K. Zhang, C. Liu, F. Huang, C. Zheng and W. Wang, *Appl. Catal., B*, 2006, **68**, 125–129.
41 A. Murphy, P. Barnes, L. Randeniya, I. Plumb, I. Grey, M. Horne and J. Glasscock, *Int. J. Hydrogen Energy*, 2006, **31**, 1999–2017.
42 R. van de Krol, Y. Liang and J. Schoonman, *J. Mater. Chem.*, 2008, **18**, 2311–2320.
43 D. Kurita, S. Ohta, K. Sugiura, H. Ohta and K. Koumoto, *J. Appl. Phys.*, 2006, **100**, 096105.
44 Z. Ma, Z. Yi, J. Sun and K. Wu, *J. Phys. Chem. C*, 2012, **116**, 25074–25080.
45 R. F. W. Bader, *Atoms in Molecules: A Quantum Theory*, Oxford University Press, New York, 1990.
46 J. Sun, X. F. Zhou, Y. X. Fan, J. Chen, H. T. Wang, X. J. Guo, J. L. He and Y. J. Tian, *Phys. Rev. B: Condens. Matter Mater. Phys.*, 2006, **73**, 045108.
47 J. Feng, X. Qian, C. Huang and J. Li, *Nat. Photonics*, 2012, **6**, 866–872.